

Chapter 9

Photocatalysis with Nanoparticles for Environmental Applications: Reactor Design Issues



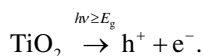
Ilenia Rossetti, Francesco Conte, Antonio Tripodi, and Gianguido Ramis

9.1 Introduction

3×10^{24} J is the annual solar irradiance, ca. 10,000 times the worldwide energy consumption [1, 2]. This strongly supports the use of solar power to drive chemical processes, either for the photocatalytic/photochemical synthesis of fuels or chemicals or for the photoconversion of noxious compounds.

The photodegradation of various pollutants has been proposed through photocatalytic processes thanks to the in situ formation of powerful oxidising species upon irradiation. Different approaches can involve homogeneous processes, such as the Photo-Fenton reaction [3] or photooxidation through UVC irradiation of H_2O_2 or heterogeneous photocatalysis. The heterogeneous photocatalytic approach has the advantage of separating and recovering the solid catalyst or using it immobilised on a separate phase with respect to the reacting mixture, limiting its impact, especially when treating wastewaters [2, 4–6].

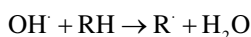
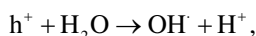
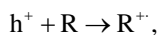
By far, the most used heterogeneous photocatalyst is TiO_2 , which can be photoexcited upon absorption of a radiation with energy larger than its bandgap. An electron is thus promoted to the conduction band of the semiconductor, leaving a hole in the valence band,



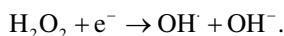
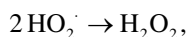
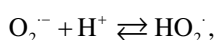
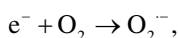
I. Rossetti (✉) · F. Conte · A. Tripodi
Chemical Plants and Industrial Chemistry Group, Dipartimento di Chimica, Università degli Studi di Milano and INSTM Unit Milano-Università, Milan, Italy
e-mail: ilenia.rossetti@unimi.it

G. Ramis
DICCA, Università degli Studi di Genova and INSTM Unit-Genova, Genova, Italy

The hole h^+ is a strong oxidant, with a Relative Oxidation Power $ROP = 2.35$ [7] and can oxidise directly an organic pollutant in water or interact with water forming hydroxyl radicals, characterised by slightly lower $ROP = 1.25$,



with R being a generic organic moiety. On the other hand, O_2 can act as electron scavenger forming a superoxide radical anion, which in turn acts as oxidant,



All the radicals so formed contribute to the oxidation of the target pollutant.

Various applications of photocatalytic oxidation processes can be found in either liquid or gas phase [8]. However, the research is mainly focussed on the development of photoactive materials, often neglecting the careful design of the photoreactor and of the relative process. This is a key point, since the reactor geometry and size, the radiation source and its distribution across the reacting medium hugely impact the photocatalytic performance, determining the success or failure of the process and posing important issues for the scale-up. Therefore, this chapter presents some different photoreactor configurations, predominantly focussing on water treatment, but dealing also in some cases with different reactions, e.g. H_2 production or CO_2 photoreduction if they present interesting reactor layouts that may suggest improvements also for water decontamination. A further section deals with modelling of different photoreactors and presents the main descriptors and mathematical approaches for their design.

9.2 Photoreactor Configurations

The main features that an efficient photoreactor should exhibit are: (1) high surface exposure of the photocatalyst per unit volume; (2) appropriate mixing and turbulence regime to ensure fast mass transfer of the reactants and efficient suspension of the catalyst in the case of slurry configuration; (3) good transparency of the solution/

suspension to radiation and (4) effective and continuous oxygen supply for oxidation reactions.

Different types of photoreactors are described in the literature. Some examples are reported in Fig. 9.1.

The most used configuration for photoreactors is the slurry one, at least in a research stage, where the catalyst is suspended in the aqueous medium containing the pollutants and irradiated either from the external surface of the reactor or through immersed lamps. This configuration has the advantage of exploiting the intrinsic activity of the catalytic material and providing optimal active site exposure to light and to the contaminant. Provided that efficient mixing conditions are achieved, it might ensure that mass transfer limitations are negligible and that statistically all the solid particles can be reached by radiation. However, a portion of the whole solid volume is shadowed by the absorption and scattering effects of the solid itself, depending on the solid particle concentration. To limit this drawback, typically small reactor volume is adopted, obtaining a more uniform radiation pattern penetrating the whole reacting volume. Furthermore, issues for scale-up and industrial exploitation arise from the need to separate and recover the catalyst after use.

A UV Free-Surface Reactor (UV-FSR) has been used for the degradation of dyes in a pilot 10 L scale [10]. It is basically a stirred tank reactor, working in continuous or batch mode, with part of its surface irradiated by one or several UV lamps. Intensive stirring throughout the process provides almost ideally turbulent conditions in the aqueous reactor content. This results in a constantly renewed surface, allowing water or contaminants to meet statistically the photon source, independent of colour and turbidity of the suspension or solution. It was tested with or without a heterogeneous photocatalyst as AOP for water treatment.

A fully new concept of high pressure slurry photoreactor, operating up to 20 bar pressure, has been developed. This prototype, with ca. 1.5 L capacity, has been used at the moment to improve the CO₂ solubility in water, boosting the reaction rate for CO₂ photoreduction and for the photoreforming of organic molecules for H₂ production [11–18]. However, the possibility to increase significantly O₂ concentration in water makes it very promising for also oxidation reactions in water treatment.

The choice between the use of suspended catalysts in a slurry arrangement or immobilised materials is hard. On one hand, a slurry configuration is preferable to maintain unaltered the intrinsic activity of the photocatalyst, since after deposition, some decrease of performance is often noticed. However, in order to achieve continuous operation when using slurry type reactors, as required for water treatment, catalyst separation, recovery and recycle are needed. A possible option is to use a selective membrane in a hybrid membrane photoreactor, as recently reviewed [5, 19]. In this arrangement, a slurry type photoreactor is used, with suitable irradiation, and a selective membrane is immersed in it to collect the clarified solution as permeate, retaining the photocatalyst in the reactor [20]. A fouling problem may arise for the membrane, since, depending on the surface charge on the photocatalyst particles, agglomeration may occur, altering the membrane properties [21]. A possible solution consists in adapting the solution pH based on surface charge measurements.

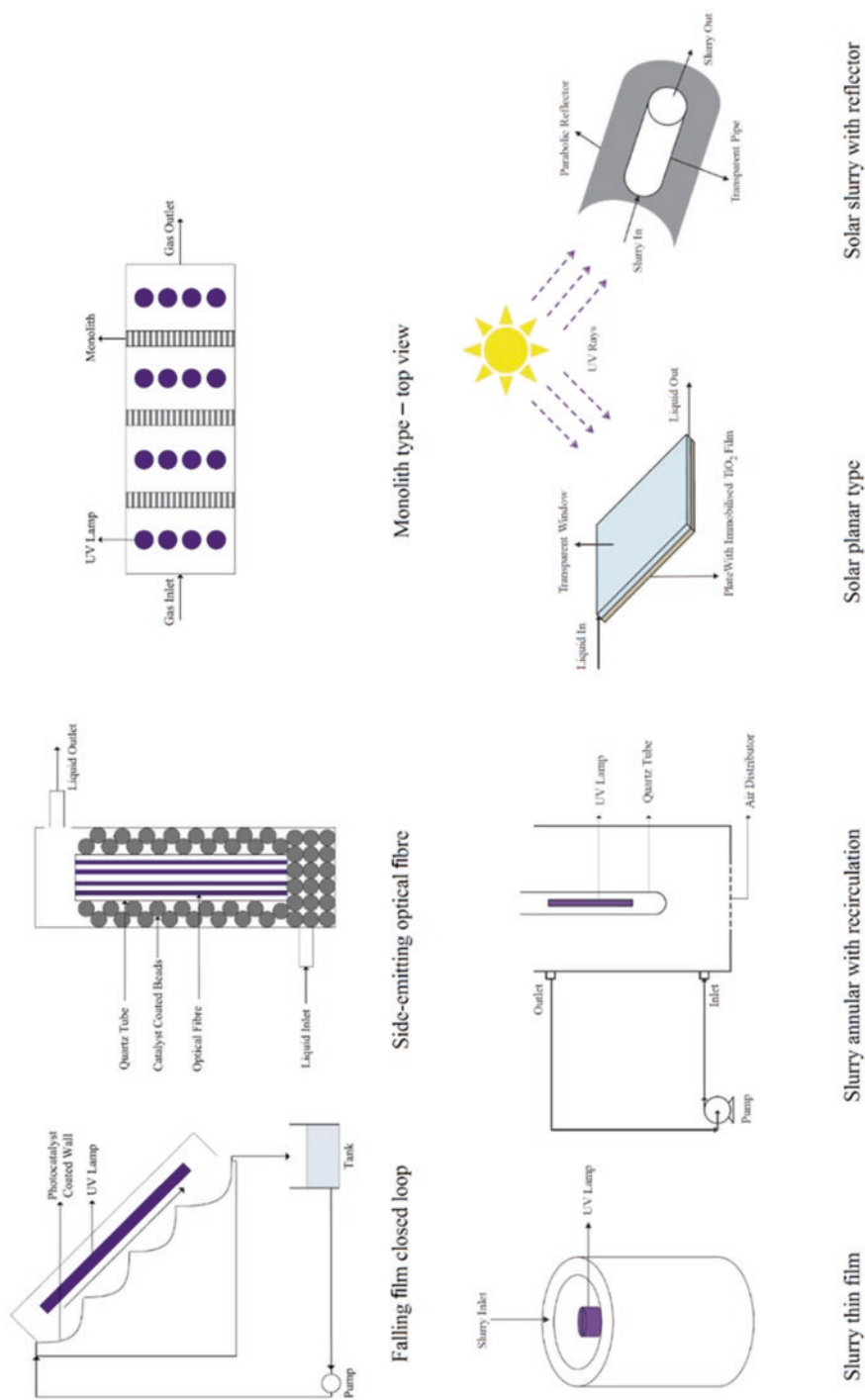


Fig. 9.1 Sketch of different photoreactor types. (Adapted and reproduced from [9] by kind permission. Copyright (2013) of Elsevier)

Different photoreactor configurations have been reviewed recently, for application to Advanced Oxidation processes (AOPs) [2]. A very simple option to overcome the limitations of slurry reactors and improve the throughput is to adopt a fixed bed configuration, which is possible by immobilisation of the active phase over a transparent material, such as glass beads [1]. However, transparency is limited and the surface interaction with the liquid is less efficient than slurry.

The possibility to use photomicroreactors, where the catalyst is immobilised in different forms over a solid substrate, allows us to overcome the downstream separation problems of the catalyst powder and to irradiate a clear and transparent solution, but also implies some limits for the decrease of active site exposure with respect to slurries.

Photocatalytic microreactors have been developed with significant surface to volume ratio ($>10,000 \text{ m}^2/\text{m}^3$) to overcome the latter limitation. Another very interesting feature that underpins the use of microreactors is that when optimised flow patterns are achieved, heat and mass transfer limitations are negligible and a uniform and predictable irradiation can be achieved [2]. Different flow patterns in three-phase microreactors are reported for the fluid flow through the microchannels, such as bubble flow [22], slug flow [23] or annular flow [24]. Microreactors can assume different shape, such as microcapillary [25], single- [26] or multi-microchannel reactors [27] or planar structure [28].

An example of capillary microreactor has been proposed by Eskandarloo et al. [26] by coating a stainless steel plate including microchannels with the photocatalyst to accomplish the oxidation of terephthalic acid under UV irradiation. Additionally, Castedo et al. [29] reported the photoproduction of H_2 with Au/TiO_2 immobilised in a silicon microreactor, which guarantees higher versatility.

Monolith-type microreactors are an interesting configuration, which consists of a regular array of channels, usually straight and coated with a thin layer of catalyst, irradiated efficiently through optical fibres located inside the channels. The fibres should not be coated to distribute uniformly the radiation across the monolith (Fig. 9.2) [30].

Different configurations have been developed. For instance, a photomicroreactor containing TiO_2 nanoparticles coated over ZnO nanorod arrays has been obtained by growing the active phase in the capillaries [31]. The assembly was used to photodegrade methylene blue. In addition, the mass and photon transfer have been improved for the reduction of Cr(VI) to Cr(III) comparing two photoreactors: a monolithic tubular photoreactor and a micro-meso-structured photoreactor, achieving in both cases a satisfactory irradiated surface to volume ratio [32]. To reduce photon transfer limitations, the tubular photoreactor was packed with transparent cellulose acetate monoliths loaded with the catalyst by dip-coating. For the other layout, a thin film was uniformly deposited on a glass slab or on a network of channels and chambers printed in the back stainless steel slab, achieving much better performance than the monolith reactor.

A completely different configuration is achieved in a twin reactor, used, e.g. to achieve the photoreduction of CO_2 by CO , which is a stronger reducing agent than water [33]. It consists of two compartments separated by an ion exchange membrane,

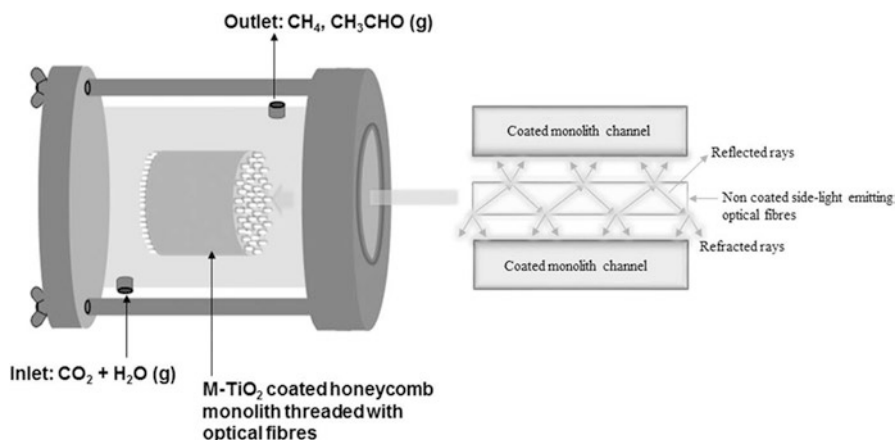


Fig. 9.2 Example of honeycomb-type micro-photoreactor, irradiated through optical fibres. (Reproduced from [30] by kind permission. Copyright (2016) Elsevier)

in the specific case allowing H^+ transfer between the two reacting sections, e.g. Nafion. The same concept has been applied to the CO_2 photoreduction assisted by H_2 evolution, where the latter is accomplished by photoreforming organic pollutants in water [1]. The same twin reactor configuration has also been applied by Baniasadi et al. [34] for the photoproduction of H_2 under visible light. Two different catalysts, one for H_2 evolution (Pt/SrTiO₃:Rh) and the other for oxygen reaction (WO₃), were separately loaded in two compartments, separated by a Nafion membrane, and using the Fe(II)–Fe(III) couple as electron transfer agent. A Compound Parabolic Concentrator (CPC) is also included. The reactor performance is not only dependent on the flow regime, needing high turbulence, but also sensitive to the high pressure drop under that conditions.

The conversion of the Direct Red 23 (DR23) dye has been successfully achieved using solar light with Fe₃O₄/TiO₂, coated on a glass tube and inserted in an annular shaped photoreactor. This assembly is also mounted in a CPC configuration and allows almost quantitative abatement of the dye [35].

A solar Offset Multi Tubular Photoreactor (OMTP) is a variant of the CPC photoreactor layout, including additional tubes in the space occupied by the axes of intersection of the CPC reflective involutes. This allows a considerable increase of the irradiated reactor volume (by 79%) and of the fluid residence time (up to 1.8 factor) with respect to a conventional CPC with the same footprint. With this assembly, the degradation efficiencies significantly increased for various pollutants [36].

A combined solar-electro-Fenton approach has been applied for the pilot scale removal of different pesticides and emerging contaminants [37]. The selected reaction is based on a redox cycle mediated by the Fe²⁺/Fe³⁺ couple, where the ferrous ions react with H₂O₂ to provide ·OH radicals as Reactive Oxygen Species (ROS). The electrochemical formation of H₂O₂ in situ avoids the handling, storage and transportation of this reactant. Furthermore, the irradiation with UVA radiation, or

better, with solar light, promotes the regeneration of Fe^{2+} with concomitant production of additional $\cdot\text{OH}$ through photoreduction of Fe^{3+} , the photodegradation of possible Fe(III)-carboxylate complexes formed as intermediates and the additional direct photolysis of the pollutants or intermediates. The pilot reactor was supplied with a CPC concentrating the solar radiation flux to the solution. The pilot scale reactor (Fig. 9.3), the largest available for this application, allowed 100 L capacity with natural solar irradiation in the facility of the Plataforma Solar de Almería (Spain). The electrochemical section of the device was constituted of four plate-and-frame electrochemical reactors, while the irradiated area was 2 m^2 for a 23 L volume of solution.

A similar reactor configuration on a pilot scale has been used for the photo-Fenton degradation of a solution of tetracyclines, which are the second largest group of antibiotics worldwide, largely excreted in water reservoirs through hospital or

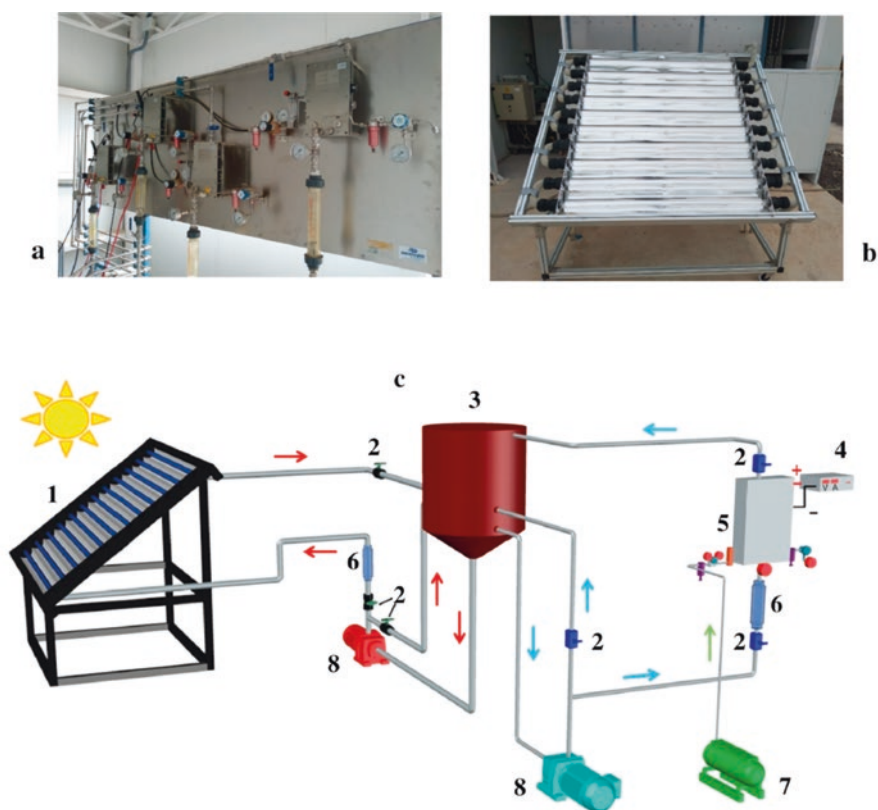


Fig. 9.3 Front view of (a) the four filter-press type electrochemical cells of the pilot unit and (b) the CPC photoreactor. In (c), schematic diagram of the pilot unit equipped with one cell (examined in this work), showing (1) CPC photoreactor, (2) valve, (3) feed tank, (4) power supply, (5) electrochemical reactor, (6) liquid flowmeter, (7) air compressor and (8) magnetic pump. (Reproduced from [37] by kind permission. Copyright (2019) by Elsevier)

domestic wastes, besides through industrial residue. Given the ineffective removal through conventional biological treatments, to avoid the insurgence of bacterial resistance, a pilot-scale photoreactor constituted of a CPC and 6 borosilicate glass tubes in series with a batch recirculating circuit was used to treat 35 L of a tetracycline solution, achieving almost 90% conversion in 2 h under different operating conditions [38]. Also, a CPC system for hydrogen production under solar light irradiation has been designed and modelled by Cao et al. [39].

A further different configuration is constituted by spinning disc reactors, which are proposed as tools for process intensification [40–43]. The reactor is composed of a spinning disc placed in the horizontal plane, which is let to rotate at different spinning velocity. The reacting mixture is injected from a central nozzle and moves towards the periphery due to centrifugal draft. The photocatalyst may be immobilised on the disc and irradiation can be achieved from top. The intensification of the process mainly occurs through a more uniform and effective penetration of light through the thin liquid layer formed over the disc and by improvement of the mass transfer coefficient. This device has been applied to the photodegradation of methylene blue and of dehydroabietic acid, a resin acid found in pulp and paper wastewater, which acts as endocrine disruptor, with adverse ecological effects even at very low concentration. The overall reaction rate has been measured at different feeding flow rates and spinning regimes, obtaining widely different results and even a change of the apparent reaction order. The latter parameter is expected as first order for most photocatalytic reactions, but it turned out to be second order for the selected applications in very specific cases. The mass balance of a Continuously Stirred Tank Reactor, perfectly mixed but unsteady due to recirculation, has been coupled with a characteristic parameter of the spinning disc device, i.e. the liquid film thickness over the disc, calculated though the Nusselt model [40]. The kinetics was interpreted in correlation with the flow pattern of the liquid on the disc. Under specific rotation speed and flow rate combinations, large standing waves were observed through a camera, disrupting in an array of irregular waves at large rotational speeds. Overall, the change in the flow structure affected the reaction rate, with the biggest intensification of mass transfer rate with the highest non-linearity of the wave pattern. However, an additional detrimental effect is due to possible scattering and modification of the light penetration in the case of large waves. The comparison of performance with an annular reactor layout revealed a significant gain of conversion of methylene blue, though at the expense of a more complex system from the mechanical point of view, due to moving parts, with consequent heavier maintenance issues [41].

In order to improve mass transfer limitations, a different configuration has also been proposed, in form of a multiblade impeller, on which the photocatalyst has been coated. This system has been named Stacked Frame Photoreactor (SFPR) and is sketched in Fig. 9.4 [44]. In this photoreactor, the propeller rotation helps mixing and thus a more efficient mass transfer with respect to immobilised photocatalytic surfaces.

An impinging jet stream photoreactor was set up with a TiO_2 -coated disc for the abatement of phenol in water. Different parameters were optimised, such as liquid

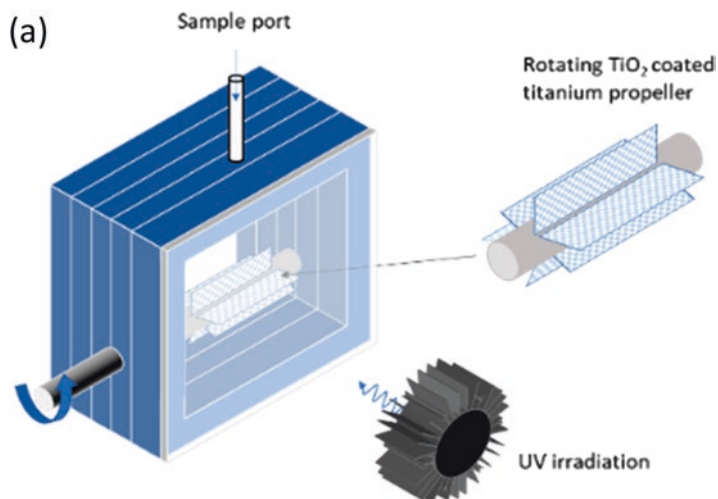


Fig. 9.4 Schematic of the SFPR with the rotating titanium propeller housed within the reactor. (Reprinted from [44] by kind permission. Copyright (2019) of American Chemical Society)

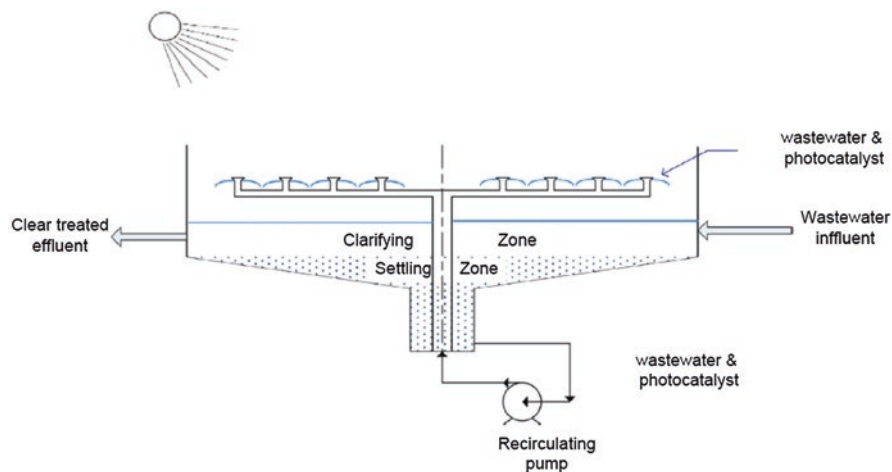


Fig. 9.5 Schematic drawing of TiO₂ “water-bell” photoreactor. (Reproduced from [48] by kind permission. Copyright (2018) by Elsevier)

flow rate, disc diameter, nozzle-to-disc distance and initial pollutant concentration. A newly developed hydrodynamic model, Langmuir-Hinshelwood kinetics and mass transfer phenomena were used to rate the system and it was compared with a spinning disc reactor, showing better performance [45–47].

A “water-bell” TiO₂-based photoreactor (Fig. 9.5) has been designed to achieve a thin water/photocatalyst film efficiently irradiated through UVA lamps, envisaging a future application with solar light [48]. The thin film has the advantage of

exchanging oxygen efficiently with surrounding air and of allowing high photocatalyst concentration, since high light penetration is not needed due to small film thickness. This also allows loading the catalyst on coarse supporting particles, to ensure easy settling and recovery of the catalyst in a so-called clarifying zone. The system is designed at a large scale as a modular set of nozzles that spray the water/photocatalyst suspension as a film to a basin for recirculation. The catalyst loading proved to be a more sensitive parameter than irradiance and the presence of an efficient electron scavenger also demonstrated important, as well as the pH.

A falling film reactor has been tested for the photodegradation of methylene blue. Ca. 4 g of TiO_2 were deposited in a four step configuration exposing ca. 0.2 m^2 surface to UVA irradiation. The mechanism of oxidation has been investigated, together with the optimisation of the reaction conditions [49]. Furthermore, falling film microreactors irradiated with LED lamps were constituted by parallel microchannels for photocatalytic-assisted synthesis [2, 50].

Similarly, Bahbani Ghatar et al. [51] investigated the same reaction in a UVA-irradiated plane falling film photoreactor based on ZnO . Also, in this case, the optimisation of the operating conditions was the objective of the work, using an experimental design over different variables: the slope of the plate, the number of lamps, their distance from the plate and the flow rate of wastewater. The combined effect of all these parameters over the observable result (dye conversion) was expressed as a function of the single parameters or combined in couples. Only some of the variables revealed particularly significant, as determined by ANOVA analysis. For instance, the distance of the lamps from the plate was not significant by itself, but the combination of distance/number of lamps and distance/water flow rate revealed important. Furthermore, the water flow rate was significant by itself and in combination with other parameters, since it can modify the film thickness of the solution and turbulence can affect the light absorbance.

The FluHelik photoreactor was used for a photochemical UVC/ H_2O_2 degradation of various emerging contaminants [52]. Tests have been carried out in both ultrapure water matrix and a real urban wastewater collected after secondary treatment. The FluHelik reactor showed 1.3 times higher mineralisation with respect to a reference reactor. Furthermore, the residual toxicity of the photodegraded products was evaluated through embryo toxicity bioassays. Furthermore, a microphotoreactor (NETmix) was used for the degradation of oxytetracycline from urban wastewater [53]. It is constituted of an array of small cylindrical chambers and prismatic transport channels and the system is assembled with a quartz slab. The optimisation of the radiation source, ensuring uniform light distribution, and the H_2O_2 concentration was performed. The same type of reactor was also used with a heterogeneous catalytic system, based on TiO_2 irradiated with a UVA source [54] and for bromate reduction [55].

The photodegradation of VOCs in air has been tested on a semi-pilot scale in a 420 L photoreactor consisting of a photocatalytic chamber that included a set of 9 W UVA fluorescent lamps and a photocatalytic filter. The latter was assembled on a cellulose-based material on which a titania-silica coating has been immobilised.

The air flow containing the pollutant was fed and recirculated to a first larger chamber, where sampling points allowed us to measure the concentration of the target molecules vs. time. The flow rate was measured before entering the photocatalytic module and air circulation was provided by a fan [56].

A summary of the different possible configurations is reported in Table 9.1.

Table 9.1 Main reactor configurations

Reactor type	Features	Advantages	Disadvantages
Slurry	Catalyst in suspension; intense mixing needed	Good surface exposure; limited mass transfer if efficient mixing is achieved	Scale-up issues; inefficient light penetration due to scattering or opaque solutions; recovery of catalyst powder
Fixed bed	Catalyst immobilised over beads	Immobilised catalyst; no recovery issues	Light penetration is inefficient
Microreactors/ capillary reactors	Catalyst immobilised in microchannels exposed to light	Good catalyst exposure to light and reactants; limited size of the channels and so limited mass transfer issues	Needed high surface to volume ratio
Monoliths	Catalyst immobilised in microchannels of a monolith exposed to light	Good surface to volume ratio; effective irradiation with LED or optical fibres in each channel	Need of complex arrangement for irradiation; complex coating procedures
Twin reactor	Separate compartments for different half reactions	Separate production of different products	Applications limited by needs of transport through a membrane; rates possibly limited for the same reason
Single or multitubular with compound parabolic collectors (CPC)	Effective collection and concentration of radiation on the tubes	Enhanced irradiation; relatively compact and simple design for multitubular systems	Sizing dependent on reaction rate
Spinning disc	Solution/suspension spread in thin film irradiated on top	Short optical path; limited mass transfer	Possible irregular flow shape; mechanically more complex due to moving parts
Stacked frame/ rotating impeller	Catalyst immobilised over rotating blades	Improved mass transfer	Mechanically more complex due to moving parts; irradiation spreading and averaging over the surface
Water bell/falling film	Solution/suspension recirculated in thin layers flowing	Improved mass transfer; effective irradiation	Need of high recirculation; intrinsically unsteady operation

9.3 Photoreactor Scale-Up and Modelling Issues

One of the key points for modelling photochemical or photocatalytic reactors is the need to include the radiation as a “pseudo-reactant” in the kinetics of the process. This allows us to integrate the characteristic equations for the reactor used (mass, momentum and heat balances) to size or rate the photoreactor. Computational methods in photocatalysis have been very recently summarised and include methods for the solution of the radiation pattern [57].

The first issue is to estimate the Local Volumetric Rate of Photon Absorption (LVRPA, e^a), i.e. a sort of “concentration of photons”. LVRPA expresses the useful photon concentration as they were reactants and thus the useful number of photons absorbed by the surface of the catalyst in the unit volume of the reactor [58].

The radiative transport equation (RTE) [59, 60] represents the most rigorous approach,

$$\frac{dI_\lambda(s, \Omega)}{ds} = -k_\lambda I_\lambda(s, \Omega) - \sigma_\lambda I_\lambda(s, \Omega) + \frac{1}{4\pi} \sigma_\lambda \int_0^{4\pi} p(\Omega' \rightarrow \Omega) I_\lambda(s, \Omega') d\Omega'$$

I_λ represents the irradiance at wavelength λ , s is a spatial coordinate and Ω represents a directional solid angle. The properties of the photocatalytic material are instead represented by an absorption coefficient k_λ and a scattering coefficient σ_λ , both depending on the wavelength. The term to be integrated $p(\Omega' \rightarrow \Omega)$ represents a scattering phase function, i.e. the probability that around the position s , a photon can be redirected from the direction Ω' to Ω . Therefore, the first term on the right represents the absorption, the second the out-scattering and the third the in-scattering of photons.

Different approaches were implemented to solve the RTE, where a rigorous Discrete Ordinate Method (DO) discretises the volume coupling and conventional mass and energy balances of Computational Fluid Dynamic (CFD) methods, with this additional radiation balance. More precisely, the knowledge of the hydrodynamics is needed to calculate the catalyst distribution in slurry reactors. CFD simulation typically solves the flow pattern, from which the time-averaged or steady state results of catalyst distribution are used to calculate the radiation field through the RTE [9].

In the case of homogeneous photoreactors, the Navier-Stokes equations are used, while for multiphase flow, an Eulerian-Eulerian (E-E) or Eulerian-Lagrangian (E-L) approach can be applied. The E-E model solves the mass and momentum balance equations for the different phases, considered as interpenetrated continua. Additional relations are needed in the case of solid phases. The E-E approach has been more frequently implemented for multiphase flows in this application [61–66]. The E-L approach simulates the trajectory of the dispersed phase particles through the equations of motion, by applying a force balance, while the continuous phase is solved through an Eulerian approach. Different turbulence models have been used for bubble columns and photocatalytic reactors, among which the κ - ϵ one, in case

accounting for bubble induced turbulence, is a good compromise between accuracy and computational demand [9]. On the contrary, for immobilised catalysts, the near-wall zone is computed by discretisation under laminar conditions.

The Discrete Ordinate (DO) model transforms the RTE, which is an integro-differential equation, into a system of algebraic equations [67, 68]. The radiation field is divided into a number of discrete directions for which the RTE is solved. Alternatively, a Finite Volume (FV) method is more flexible with respect to geometries, while the DO can span the whole optical thickness, has dedicated non-grey models and has been successfully applied to both immobilised and slurry photoreactors. A very nice example of application of CFD modelling to photoreactor design is proposed by Boyjoo et al. [66], where a DO approach is used, also implemented as a FV method in a commercial software for CFD, such as Fluent®. The reaction order with respect to the LVRPA showed variable depending on light intensity, i.e. 0.5 at high irradiance (due to more frequent parasitic electron-hole recombination events) and 1 for low irradiance. Following an E-E model, the phases are modelled as interpenetrating continua for the solution of the mass and momentum conservation balances. The rate of reaction is expressed as

$$-r_p = kf(c_p)LVRPA^m,$$

where $m = 0.5-1$ depending on the regimes and $f(c_p)$ was a function of the concentration of pollutant to be treated corresponding to a first order kinetics or a Langmuir-Hinshelwood expression. The radiation modelling was carried out through DO modelling, by dividing the radiation field into discrete directions and solving the RTE separately for each of them. The FV tool in Fluent® was also used, by discretising each control volume (e.g. 72 solid angles). However, the simultaneous solution of the radiation field and the fluid dynamics is not currently possible in the commercial tool. So, at first, the simulation was made on the phases, getting the mean catalyst concentration and velocity vectors. Then, the radiation was modelled, accessing the catalyst local concentration data previously stored, to calculate the optical properties of the medium and LVRPA. The latter was then used to model the reaction rate and, consequently, the reactor balances. Different photoreactor layouts were tested, holding 1, 2 or 4 lamps, with optimised, different grids for the fluid dynamic simulation and the radiation modelling [66].

CFD modelling was also applied to the SFPR reactor depicted in Fig. 9.4 using a rotating machinery turbulent flow $\kappa\text{-}\epsilon$ model [44]. The rays emitted by a LED lamp were modelled as deriving from a point source and so, depending on the distance from the TiO₂-coated propeller, the amount of radiation reaching the surface was calculated. As reasonable, the latter parameter decreased upon increasing the distance from the lamp. However, another important feature was highlighted through the model. It was previously reported that rapidly switching LED sources can improve the activity due to more controlled excitation, which would decrease the recombination of the photogenerated charges [44, 69–71]. This effect can be achieved through the rotation of the propeller, which alternates the surfaces exposed

to light. The calculated irradiance at different lamp-reactor distance and with different positions of the propeller is exemplified in Fig. 9.6. The effect of the lamp distance from the photocatalyst layer is immediately evident between 4 cm (Fig. 9.6a, b) and 7 cm (Fig. 9.6c, d). The shadowing zones are also evidenced during the rotation of the photocatalyst.

Similarly, a CFD approach allowed us to optimise the configuration of a UV LED array, tested for the photodegradation of cinnamic acid as model for agro-industrial waste water [72]. LEDs may be usually represented as point sources and can now reach high intensity irradiance, which makes the reaction rate order with respect to radiation intensity non-linear. Thus, the accurate prediction of light distribution (again with fluid dynamic assessment of catalyst and reactant distribution across the reactor) is a fundamental task for optimisation. Different reactor geometries were also tested [73].

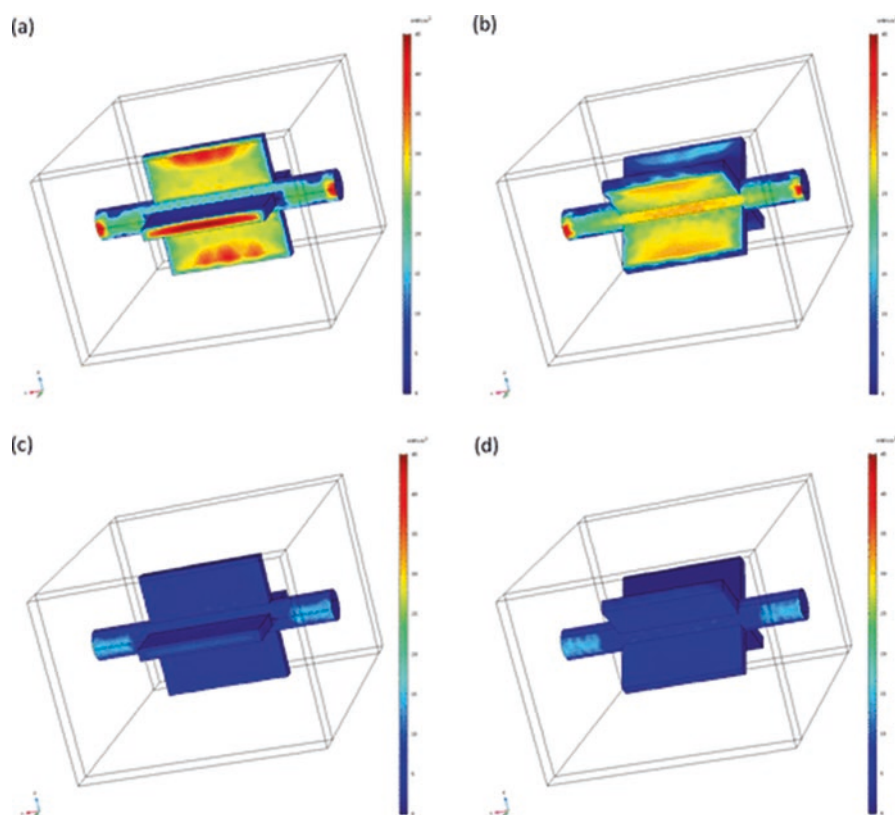


Fig. 9.6 3D surface plots of the irradiance on the catalyst surface at 4 cm lamp/reactor distance in both the initial configuration (a) and the rotated propeller position (b) or at 7 cm distance in the initial static position (c) and the rotated propeller one (d). (Reproduced from [44] by kind permission. Copyright (2019) by American Chemical Society)

The best piping arrangement in a pilot annular photoreactor has been modelled, considering a FluHelik reactor and a conventional Jet reactor. The residence time and radiation distribution have been calculated by CFD for the degradation of 3-amino-5-methylisoxazole with H_2O_2 /UVC and UVC processes [74].

Various reactor layouts were modelled through CFD. For instance, as a non-exhaustive list, a channelled optical fibre reactor was applied to ethylene photodegradation in gas phase [75] and for its oxidation in non-ideal fixed bed flow reactors [76]; a baffled flat plate photoreactor irradiated with UVA-LED was used for the degradation of $Fe(CN)_6^-$, a recalcitrant compound present in mining wastewaters [77]; the FV module implemented in Fluent[®] was used to model a single phase annular photoreactor [78]; an annular photocatalytic reactor to degrade Rhodamine B was simulated using Fluent[®] [79]; the photodegradation of acetaldehyde in air has been modelled in a multi-tubular reactor [80].

Alternatively, a Monte Carlo (MC) stochastic approach can be used to solve the RTE. For both the DO and MC approaches, the rigorous solution is obtained at the expense of computational cost, so that typically, these methods are employed for constant irradiance sources, such as lamps, avoiding solar photoreactors for which the variation of the input source would be scarcely manageable.

The MC method [58] is based on the random scattering and absorption phenomena (Fig. 9.7, right), which can be modelled in a slab reactor through the definition of a grid of thickness dx and by correlating the trajectory of each photon in the slab through an array R of numbers, which assumes random values between 0 and 1. A mean free path (l) of the photon is defined as the free pathway between two consecutive absorption or scattering events. This is correlated with the extinction coefficient of the suspension (β) as

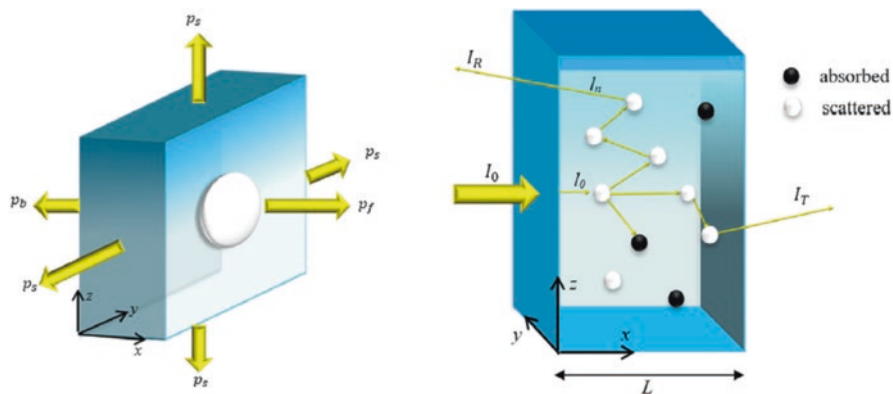


Fig. 9.7 Left: Scattering directions considered by the SFM in a differential volume of liquid containing a particle. Right: schematic diagram of the slab photoreactor with absorbing and scattering particles suspended in the inside. I_0 , I_R and I_T are the incident, reflected and transmitted intensity of light, L is the reactor length and l the free path of photons. (Reproduced from [58] by kind permission. Copyright (2016) by Elsevier)

$$l = -\frac{1}{\beta} \ln R,$$

l and the direction θ_i where the photon is emitted allow the calculation of the new position (x_i) of the photon, which should lie between 0 and L ; otherwise, the photon exits the slab and it is no more useful,

$$x_i = x_{i-1} + l \cos \theta_i.$$

When the free path is passed, the photon is absorbed or scattered based on the value of R : the photon is absorbed and its location recorded if $R \geq \omega$, where ω is defined as the scattering albedo, i.e. the ratio between the scattering and the extinction coefficients, defining the scattering probability. If $R < \omega$, the photon is scattered towards a new random direction, whose longitude and latitude angles (azimuth α and zenith φ , respectively) are found randomly in the range $[0; 2\pi]$. φ is expressed as a function of R and of the phase function, while the azimuth as

$$\alpha_{i+1} = 2\pi R.$$

Finally, the scattering angle is

$$\cos \theta_{i+1} = \cos \varphi_{i+1} \cos \theta_i + \sin \varphi_{i+1} \cos \alpha_{i+1} \sin \theta_i.$$

The radiative heat transfer in a multi-channel solar reactor was performed through MC on a single channel level [81]. A coating of ZnFe_2O_4 was considered to optimise the channel geometry and film thickness.

Another alternative approach is the Six Flux Absorption-Scattering Model (SFM), which provides a simplified solution adequate for most practical purposes. The latter has been proposed for homogeneous photoreactors by Brucato et al. [82], with pioneering simplified models to predict radiation distribution in various reactor layouts [83–87]. The SFM model admits scattering in the six directions of a Cartesian space, defined as forward (f), backward (b) and sideward (s), with relative probability p_i ($i = \text{f,b,s}$) (Fig. 9.7). p_i depends on the phase function for scattering and has been variously calculated depending on the type of scattering that is assumed [58, 82, 88, 89]. For heterogeneous photocatalysts, the determination of the absorption and scattering coefficients is a fundamental step for the reliability of the model and some estimates of the relevant parameters for TiO_2 is reported by Acosta-Herazo et al. [58], together with a very effective comparison between the MC and SFM approaches.

A SFM approach has been used to evaluate the LVRPA in a planar photoreactor, distinguishing the radiation fraction in UVA and Vis regions when coupling materials able to absorb different spectral ranges and therefore, they contribute differently to absorption and scattering. In the case of polychromatic sources, such as solar radiation, the photoactive materials should be carefully analysed to predict their

optical properties and to calculate the relevant parameters. In the example reported by Acosta-Herazo et al. [90], TiO_2 absorbs and scatters light in the UVA region, while goethite absorbs both UVA and part of the Visible spectrum. The SFM is therefore applied to polychromatic radiation and the net radiation absorbed by the goethite photocatalyst was calculated summing the contributions from the UVA and the Visible radiation. So the net radiation absorbed by goethite was calculated summing both contributions,

$$e_{\text{TiO}_2}^a(x) = e_{\text{UVA}}^a(x) \left(\frac{\text{W}}{\text{m}^3} \right),$$

$$e_{\text{goethite}}^a(x) = e_{\text{UVA}}^a(x) + e_{\text{Vis}}^a(x) \left(\frac{\text{W}}{\text{m}^3} \right).$$

The optical properties of both materials were averaged in the relevant spectral range and depend on catalyst concentration, e.g.

$$\kappa^* = \frac{\int_{\lambda_{\min}}^{\lambda_{\max}} \kappa_{\lambda}^* I_{\lambda} d\lambda}{\int_{\lambda_{\min}}^{\lambda_{\max}} I_{\lambda} d\lambda} \left(\frac{\text{m}^2}{\text{kg}} \right),$$

$$\sigma^* = \frac{\int_{\lambda_{\min}}^{\lambda_{\max}} \sigma_{\lambda}^* I_{\lambda} d\lambda}{\int_{\lambda_{\min}}^{\lambda_{\max}} I_{\lambda} d\lambda} \left(\frac{\text{m}^2}{\text{kg}} \right),$$

$$g = \frac{\int_{\lambda_{\min}}^{\lambda_{\max}} g_{\lambda} I_{\lambda} d\lambda}{\int_{\lambda_{\min}}^{\lambda_{\max}} I_{\lambda} d\lambda} (-),$$

where κ is the absorption coefficient, σ is the scattering coefficient, while g is a parameter used to compute the phase function (e.g. defined according to Henyey-Greenstein, but different approaches are also reviewed in [9]). The limits for integration depend on the absorption edge of each material.

The optical thickness of an absorbing medium can also be calculated, assuming a characteristic length L of the system (e.g. slab length or annulus thickness), as [9]

$$\tau_{\text{abs}} = \kappa_{\lambda} L.$$

The particle agglomeration, if occurring near the isoelectric point of the material, can also be an issue, which is accounted for by correcting the extinction coefficient (β) with respect to aggregation,

$$\beta_{\lambda}^* = \kappa_{\lambda}^* + \sigma_{\lambda}^*,$$

$$\beta_{\text{aggr},\lambda}^* = \beta_{\lambda}^* \frac{\ln T(t, W_{\text{cat}})}{\ln T(t_1, W_{\text{cat}})},$$

$$\sigma_{\text{aggr},\lambda}^* = \beta_{\text{aggr},\lambda}^* - \kappa_{\lambda}^*,$$

where t_1 is the time in which the suspension is formed and T is the transmission, depending on catalyst concentration (W_{cat}) and, in the case of particles aggregation, on time t ,

$$T(t, W_{\text{cat}}) = \frac{\text{Transmitted radiation flux at time } t \text{ and catalyst loading } W_{\text{cat}}}{\text{Transmitted radiation flux at time } t \text{ and pure water}}.$$

Different parameters have been introduced to analyse and compare the performance of photoreactors, such as the Initial Rate of Photon Absorption (IRPA),

$$\text{IRPA} = - \left[\frac{d}{dx} (e^a(x)) \right]_{x=0},$$

which may result in the following equation:

$$\text{IRPA} = -I_0 c_{\text{cat}}^2 \psi \left(\frac{W}{\text{m}^4} \right),$$

$$\psi = (\beta^*)^2 \frac{a^2 (1 - \omega_{\text{corr}}^2)}{(1 - \gamma) \omega_{\text{corr}}} \left[\gamma \left(\omega_{\text{corr}} - 1 - \sqrt{1 - \omega_{\text{corr}}^2} \right) - \left(\omega_{\text{corr}} - 1 + \sqrt{1 - \omega_{\text{corr}}^2} \right) \right]$$

with $\beta^* = \sigma^* + \kappa^*$ being specific extinction coefficient. The IRPA is very sensitive to catalyst concentration and thus, the optimal catalyst amount has to be calculated depending on its optical properties and be in turn related to the reactor thickness L to maximise the absorption of the incoming radiation.

Another useful indicator is the Total Rate of Photon Absorption (TRPA), which quantifies the total radiation absorbed in the whole volume,

$$\frac{\text{TPRA}}{A} = \int_0^L e^a(x) dx.$$

Also, in this case, useful parameters relative to TiO_2 are reported by Acosta-Herazo et al. [90].

The SFM approach has also been used to model the LVRPA in a CPC photoreactor for the abatement of acetaminophen, a hugely used drug [91], by using a Langmuir-Hinshelwood kinetic expression. The reactor mass balance has been solved as a series of plug-flow and continuous stirred reactors to treat 5000 L of wastewater (daily amount of a medium-size Colombian hospital).

Different lamp models were proposed, as line source, surface or volume emitters [9], whose equations are summarised in the cited reference.

In the case of immobilised photocatalysts (planar coatings, monoliths, etc.), there is no scattering and absorption at difference with slurry systems (if a clear and transparent medium is treated). In this case, the RTE is calculated through the Beer-Lambert equation where the incident light on the photocatalyst surface (I_0) is calculated by subtracting the reflected part from the inlet radiation intensity ($I_0 = I_{in} - I_r$). Possibly, some scattering may be due to air bubbles, if present [9].

Once the model for the source and the integration of the RTE gives quantitative indications on the useful radiation amount available as a “pseudo-reactant”, the kinetic equation can be derived. At first, intrinsic kinetics is considered, i.e. neglecting the possible physical limitations due to mass transport in the fluid phase or in the porous solid particles. Subsequently, these factors should be added.

In general, the kinetic equation can be written as a function of the concentration of the reactants, usually the pollutant concentration in the case of water treatment. The function is commonly first order or expressed in Langmuir-Hinshelwood form,

$$-r = kf(c_i),$$

$$k = f(\text{pH}, T, c_{\text{O}_2}, W_{\text{cat}}, \text{LVRPA}).$$

The dependence on the radiation intensity is often expressed through a “reaction order” of the LVRPA, which depends on different parameters, as reviewed elsewhere [9]. Furthermore, photon absorption with varying catalyst concentration has been modelled by Cao et al. [92].

A generalised model was developed to rate solar CPCs with different arrangement for degradation of water pollutants. A modified Langmuir–Hinshelwood kinetics has been developed, together with a new model to quantify the “effective” quantum yield. It is computed from the optical properties of the catalyst and the incident photon flux, without dependence on the composition, the operating conditions, the geometry and the scale of the reactor [93].

The RTE has been integrated with a Dirichlet boundary condition on the film surface exposed to irradiation, [60]

$$\frac{dI_\lambda(s)}{ds} = -k_\lambda I_\lambda(s).$$

$$I_{\lambda,s} = I_{\lambda,0}.$$

It can be integrated to yield

$$I_{\lambda,s} = I_{\lambda,0} e^{-k_\lambda s}.$$

The mass transport of each species has been modelled under steady state conditions according to Fick's first law, as diffusive flux N_i ,

$$N_i = -D_{\text{eff}} \nabla c_i,$$

$$D_{\text{eff}} = \frac{D_j \varepsilon}{\tau}.$$

Take into account the effective diffusivity D_{eff} as a function of the diffusion coefficient of species i in the reaction medium j ($D_{i,j}$), the porosity (ε) and the tortuosity factor (τ) of pores constituting the photocatalyst.

Accordingly, the rate of conversion of species i was defined assuming a first order dependence on concentration and an order γ on light intensity, as

$$r_i = -\eta k_{r,\text{app}} c_i I_{\lambda,s}^\gamma (1 - \varepsilon).$$

The effectiveness of the catalyst (η) has been conventionally defined as

$$\eta = \frac{\tanh(\phi)}{\phi},$$

where the Thiele modulus for a first order reaction was formulated as

$$\phi = (\delta - y) \sqrt{\frac{k_{r,\text{app}} I_{\lambda,0}^\gamma}{D_{\text{eff}}}},$$

representing as usual the ratio between the potential rate of reaction and that of diffusion inside the pores of the solid. A discussion on the suggested values for the various parameters can be found in [60] and references therein. The adopted model neglects diffusional limitations in the liquid phase, which is reasonable for monolith or microchannel photoreactors operating at high Reynolds number. The normalised reaction rate (r/r_{max}) was modelled depending on the thickness of the photocatalyst coating for the two front side (FSI) and back side (BSI) irradiation (Fig. 9.8b, c). The study returned the optimal value of the thickness for both cases and the attenuation of light intensity depending on the latter parameter. A correlation for film thickness optimisation depending on the various operating parameters was also proposed [60].

Additionally, CO₂ photoreduction has been investigated in the presence of a more powerful reducing agent than H₂O, studying the effect of different operating parameters in a twin reactor to predict the productivity of methanol under natural irradiance exposure [33]. A model for the reactor has been derived considering the reaction rate as a function of irradiance, where higher m exponents mean a better utilisation of photons in the given reactor geometry,

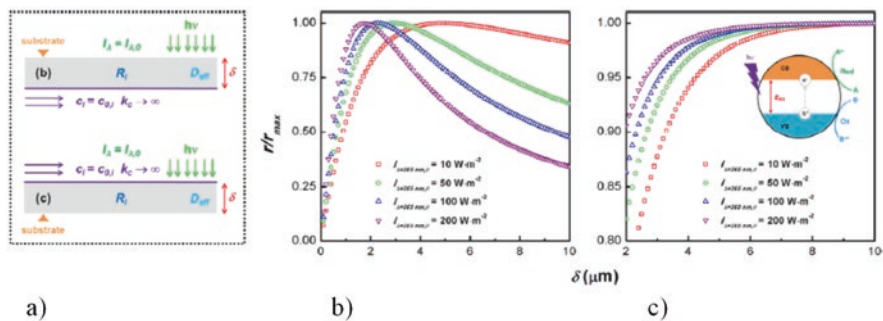


Fig. 9.8 (a) Top, Back Side (BSI) and bottom, Front Side (FSI) Irradiation of photocatalyst coating. (b, c) Normalised reaction rate vs. photocatalyst film thickness (δ) for BSI and FSI arrangement, respectively. (Reproduced from [60] by kind permission. Copyright (2017) by Elsevier)

$$r_j = I^m \left(k_j \prod_{i=1}^n c_i^{v_i} \right).$$

Mass transfer was computed according to the two-film theory and the solubility following Henry’s coefficient, calculated keeping into account the effect of the ionic strength of the solution. Sunlight was modelled using dedicated software. It was concluded that temperature and pressure were determinant factors to improve the mass transfer coefficients and gas solubility in water, respectively [13, 16, 17].

The optimal photocatalyst layer thickness has been calculated for the degradation of methylene blue as model reaction in microphotoreactors [60]. The comparison between two irradiation modes in immobilised catalyst layers, i.e. BSI or FSI, was compared, developing a radiation model to be included in the reaction kinetics. The fluid dynamic properties of the fluid in the channel were also considered. In the BSI arrangement, the maximum incident radiation and the maximum pollutant concentration occur on the opposite side of the assembly, while in FSI, they occur on the same side of the photocatalytic film (as they were in a counter- or co-current arrangement, respectively) (Fig. 9.8).

A similar comparison was done for the gas phase photodegradation of *n*-decane as model compound for VOCs. In such a case, however, no significant difference between FSI or BSI illumination was noticed, thanks to the high porosity of the catalytic layer and high diffusivity of the reactant [94].

Kinetic modelling has been considered by Charles et al. [95] in a microreactor assuming a Langmuir-Hinshelwood expression to represent the degradation of salicylic acid, with K being the adsorption constant of the compound to oxidise and C_s its surface concentration,

$$r = \frac{kKC_s}{1 + KC_s}.$$

The residence time distribution was evaluated in the microreactor with the auxilium of an inert tracer and compared with a plug-flow reactor. The mass transfer coefficient $k_{m,ext}$ has been calculated through the Sherwood number (Sh), thanks to an existing correlation developed by Ergu et al. [95, 96] as a function of the Reynolds (Re) and Schmidt (Sc) numbers,

$$\text{Sh} = \frac{k_{m,ext} d_h}{D},$$

$$\text{Re} = \frac{\rho u d_h}{\mu},$$

$$\text{Sc} = \frac{\mu}{\rho D},$$

$$\text{Sh} = 2.076 \times \text{Re}^{0.28} \left(\frac{L}{d_h} \right)^{-0.12} \times \text{Sc}^{0.33},$$

where μ is the fluid viscosity, ρ its density, u the linear velocity, D the diffusion coefficient and d_h the characteristic length of the system, e.g. the channel hydraulic diameter.

Different arrangements of micro- and meso-photoreactors have been proposed, either for scale-up or numbering-up purposes [97] for the degradation of dyes or organic pollutants. The flow systems have been characterised according to the flow rate, Reynolds, Damköhler and Peclet numbers, also identifying the definition of pertinent efficiency quantifiers. At first, the irradiance (I) has been simply defined as dependent on the optical absorbance of the medium, obtained multiplying the extinction coefficient ε , the concentration of the absorbing species c and the optical path (l). The incident radiation I_0 can be measured through a radiometer,

$$I = I_0 e^{-\varepsilon c l}.$$

The authors considered strictly laminar flow regimes. The second Damköhler (Da_{II}) number was calculated considering the ratio between the reaction and the mass transfer rates as

$$\text{Da}_{II} = \frac{\text{reaction rate}}{\text{diffusive mass transfer rate}} = \frac{k'' H}{D}$$

with H being the channel height and $k'' = k(V/A)$ the reaction rate constant corrected by the ratio between the reactor volume and surface area of the catalyst. In addition, the Peclet (Pe) number is introduced to quantify the relative roles of advection and diffusive mass transport, with L being the characteristic length for advection [97],

$$Pe = \frac{\text{diffusion time}}{\text{advection time}} = \frac{H^2/D}{L/u}$$

To quantify the efficiency of the process, different concepts can be used. According to IUPAC, the correct statement of quantum yield would be the ratio between the number of reactive events and the number of photons absorbed, which are impractical to determine. A more direct parameter is defined as apparent quantum yield, which compares the rate of conversion of the target molecule with the rate of photons incident on the catalyst surface. However, other indexes of efficiency may be related to the energy consumption to degrade a given amount of pollutant. For instance, IUPAC defined the Electrical Energy per Order (E_{EO}) as the electrical energy required for the degradation of a contaminant by one order of magnitude, in a unit reactor volume of wastewater [97, 98] for both batch and continuous flow operation (P is the power consumption, t the time, V the reactor volume and F the volumetric flow rate),

$$E_{EO\text{-Batch}} = \frac{1000 \times P \times t}{V \times \log\left(\frac{c_0}{c_t}\right)} \quad \text{or} \quad E_{EO\text{-Continuous}} = \frac{P}{F \times \log\left(\frac{c_0}{c_t}\right)}$$

Alternatively, a Reactor Characterisation (R_c) number has been introduced as a factor for selecting the best UV source from an economic point of view during dye degradation in a pilot scale photoreactor [10],

$$R_c = \frac{\text{input power (W)} \times \text{UV-C efficiency (\%)}}{\text{Reactor Volume (L)}}$$

As said, homogeneous Fenton or Photo-Fenton approach can be used to abate pollutants from waste water [3, 99, 100]. The kinetic model of this reaction, applied to the oxidation of paracetamol, has been proposed including a form of LVRPA. The kinetic expression was expressed as.

$$[\mathbf{R}(x,t)] = [\mathbf{R}^T(x,t)] + \Phi \sum_{\lambda} e_{\lambda}^{\alpha}(x,t) \tau(x,t),$$

where $\mathbf{R}(x,t)$ is the vector of formation/conversion rates of each product/reactant, $\mathbf{R}^T(x,t)$ is the contribution to the rate of thermal (dark) reactivity, Φ is the quantum yield averaged over the wavelength and the summation computes the LVRPA in polychromatic conditions. $\tau(x,t)$ is the term that completes the expression of the reaction rates, as detailed in [101].

This expression of the rate is therefore included in the mass balance of the reactor, setting $C = C^0$ at $t_0 = 0$ as initial condition and considering the volume averaged quantity indicated between $\langle \rangle$,

$$\frac{dC}{dt} = R^T(t) + \frac{V_{\text{IRR}}}{V_{\text{TOT}}} \Phi \sum_{\lambda} e_{\lambda}^a(x,t) \tau(x,t).$$

To compute the spatial distribution of the radiation, a line source radiation model was introduced, assuming a spherical and isotropic emission,

$$e_{\lambda}^a(x,t) = \kappa_{\lambda}(x,t) \frac{P_{\lambda,s}}{2\pi L_L} \int_{\theta_1}^{\theta_2} \exp\left[-\frac{\kappa_{T,\lambda}(x,t)(r_i - r_{\text{int}})}{\cos\theta}\right] d\theta,$$

where $P_{\lambda,s}$ is the lamp emission power, $\kappa_{\lambda}(x,t)$ and $\kappa_{T,\lambda}(x,t)$ are the volumetric absorption coefficient of the reacting species and of the medium, respectively, r the radius and L_L the useful length of the lamp [101].

The overall quantum yield is a parameter that can allow the comparison of different catalysts and to assess the overall feasibility of the photocatalytic process. It may be calculated as the ratio between the pollutant degradation reaction rate and the LVRPA (both volume averaged) [9].

An interesting definition of energy and exergy balances has been proposed [34], though for the photoproduction of H_2 and not for the abatement of pollutants. At first, the irradiance of solar light was determined as follows: K_{λ} measures monochromatic intensity of the radiation and n represents the numbering of intervals of wavelengths selected,

$$j_s = 4.329 \times 10^{-5} \pi \sum_n (K_{\lambda} \Delta\lambda)_n,$$

$$q_e = \alpha_s \varepsilon_b (T^4 - T_0^4),$$

where q_e is the energy exchanged between the reactor and the surroundings, α_s is the absorptivity of the reactor surface and ε_b is the Boltzmann constant. The energy efficiency of the process has been calculated as

$$\eta = \frac{n_{H_2} \text{HHV}_{H_2}}{\gamma [\alpha_v j_v + \alpha_{nv} (j_s - j_v)] + n_{H_2O} h_{H_2O} + 0.5 V_{H_2O,in}^2}$$

with γ being radiation weakening factor, α_v and α_{nv} the absorptivity of the catalyst in the visible region and the non-visible one, n the moles of each compound, HHV the higher heating value, V the volume and j_v the irradiance in the visible range. The results revealed the highest efficiency at the minimum visible light absorptivity and a significant energy and exergy loss when increasing the temperature, suggesting the need of an efficient heat exchange system.

The modelling of falling film reactors has been accomplished under turbulent flow regime considering a pilot scale photoreactor, 1.25 m \times 1 m in size [102]. Different papers considered a laminar regime, but in order to keep the photocatalyst

in suspension, turbulence was needed, with $Re > 15,000$. This induces waves to be statistically described since they determine the falling film thickness and, hence, the absorption of radiation by the suspension. The velocity profiles were then estimated by momentum balances and the LVRPA was solved according to a SFM approach.

9.4 Conclusions

The scale-up of photochemical or photocatalytic reactors is a required step to exploit advanced oxidation processes and similar remediation processes to treat water effluents. Besides searching for active materials, it is important to describe reactor geometry, flow patterns and solid properties in order to understand the interaction between the reactants, the catalyst and the third actor, i.e. radiation.

Different reactor layouts are available, yet conceptualised at a pilot scale, to maximise the exposure to solar light and to limit mass transfer and radiation distribution issues. Various modelling tools are also available to describe the reaction rate as dependent on reactants, catalyst and radiation distribution across the photoreactor.

Broader efforts are needed for radiation modelling and its coupling to reactor design. Specific attention should be put on microreactor devices and on those configurations, which reached a pilot scale development to allow validation and further improvement.

Tools which couple CFD with radiation modelling should be implemented to provide rigorous methods to scale-up photoreactors.

References

1. V.H. Nguyen, J.C.S. Wu, Recent developments in the design of photoreactors for solar energy conversion from water splitting and CO₂ reduction. *Appl. Catal. A Gen.* **550**, 122–141 (2018). <https://doi.org/10.1016/j.apcata.2017.11.002>
2. D. Heggo, S. Ookawara, Multiphase photocatalytic microreactors. *Chem. Eng. Sci.* **169**, 67–77 (2017). <https://doi.org/10.1016/j.ces.2017.01.019>
3. F.S. Freyria, M. Compagnoni, N. Ditaranto, I. Rossetti, M. Piumetti, G. Ramis, B. Bonelli, Pure and Fe-doped mesoporous titania catalyse the oxidation of acid orange 7 by H₂O₂ under different illumination conditions: Fe doping improves photocatalytic activity under simulated solar light. *Catalysts* **7**, 213 (2017). <https://doi.org/10.3390/catal7070213>
4. S. Mozia, Photocatalytic membrane reactors (PMRs) in water and wastewater treatment. A review. *Sep. Purif. Technol.* **73**, 71–91 (2010). <https://doi.org/10.1016/J.SEPPUR.2010.03.021>
5. R. Molinari, C. Lavorato, P. Argurio, Recent progress of photocatalytic membrane reactors in water treatment and in synthesis of organic compounds. A review. *Catal. Today* **281**, 144–164 (2017). <https://doi.org/10.1016/J.CATTOD.2016.06.047>
6. R. Molinari, C. Lavorato, P. Argurio, K. Szymański, D. Darowna, S. Mozia, Overview of photocatalytic membrane reactors in organic synthesis, energy storage and environmental applications. *Catalysts* **9**, 239 (2019). <https://doi.org/10.3390/catal9030239>

7. R. Munter, Advanced oxidation processes—current status and prospects. *Proc. Est. Acad. Sci. Chem.* **50**, 59–80 (2001)
8. Y. Boyjoo, H. Sun, J. Liu, V.K. Pareek, S. Wang, A review on photocatalysis for air treatment: from catalyst development to reactor design. *Chem. Eng. J.* **310**, 537–559 (2017). <https://doi.org/10.1016/j.cej.2016.06.090>
9. Y. Boyjoo, M. Ang, V. Pareek, Some aspects of photocatalytic reactor modeling using computational fluid dynamics. *Chem. Eng. Sci.* **101**, 764–784 (2013). <https://doi.org/10.1016/j.ces.2013.06.035>
10. E. Bahadori, M. Rapf, A. Di Michele, I. Rossetti, Photochemical vs. photocatalytic azo-dye removal in a pilot free-surface reactor: is the catalyst effective? *Sep. Purif. Technol.* **237**, 116320 (2020). <https://doi.org/10.1016/j.seppur.2019.116320>
11. G. Ramis, E. Bahadori, I. Rossetti, Photoreactors design for hydrogen production. *Chem. Eng. Trans.* **74**, 481–486 (2019). <https://doi.org/10.3303/CET1974081>
12. M. Compagnoni, G. Ramis, F.S. Freyria, M. Armandi, B. Bonelli, I. Rossetti, Innovative photoreactors for unconventional photocatalytic processes: the photoreduction of CO₂ and the photo-oxidation of ammonia. *Rend Lincei* **28**, 151–158 (2017). <https://doi.org/10.1007/s12210-017-0617-z>
13. F. Galli, M. Compagnoni, D. Vitali, C. Pirola, C.L. Bianchi, A. Villa, L. Prati, I. Rossetti, CO₂ photoreduction at high pressure to both gas and liquid products over titanium dioxide. *Appl. Catal. B Environ.* **200**, 386–391 (2017). <https://doi.org/10.1016/j.apcatb.2016.07.038>
14. A. Olivo, E. Ghedini, M. Signoretto, M. Compagnoni, I. Rossetti, Liquid vs. gas phase CO₂ photoreduction process: which is the effect of the reaction medium? *Energies* **10**, 1394 (2017). <https://doi.org/10.3390/en10091394>
15. I. Rossetti, A. Villa, M. Compagnoni, L. Prati, G. Ramis, C. Pirola, C.L. Bianchi, W. Wang, D. Wang, CO₂ photoconversion to fuels under high pressure: effect of TiO₂ phase and of unconventional reaction conditions. *Cat. Sci. Technol.* **5**, 4481–4487 (2015). <https://doi.org/10.1039/C5CY00756A>
16. E. Bahadori, A. Tripodi, A. Villa, C. Pirola, L. Prati, G. Ramis, N. Dimitratos, D. Wang, I. Rossetti, High pressure CO₂ photoreduction using Au/TiO₂: unravelling the effect of the co-catalyst and of the titania polymorph. *Cat. Sci. Technol.* **9**, 2253–2265 (2019)
17. E. Bahadori, A. Tripodi, A. Villa, C. Pirola, L. Prati, G. Ramis, I. Rossetti, High pressure photoreduction of CO₂: effect of catalyst formulation, hole scavenger addition and operating conditions. *Catalysts* **8**, 430 (2018). <https://doi.org/10.3390/catal8100430>
18. I. Rossetti, A. Villa, C. Pirola, L. Prati, G. Ramis, A novel high-pressure photoreactor for CO₂ photoconversion to fuels. *RSC Adv.* **4**, 28883–28885 (2014). <https://doi.org/10.1039/c4ra03751k>
19. C.S. Ong, W.J. Lau, P.S. Goh, B.C. Ng, A.F. Ismail, Investigation of submerged membrane photocatalytic reactor (sMPR) operating parameters during oily wastewater treatment process. *Desalination* **353**, 48–56 (2014). <https://doi.org/10.1016/j.desal.2014.09.008>
20. R.A. Damodar, S.J. You, S.H. Ou, Coupling of membrane separation with photocatalytic slurry reactor for advanced dye wastewater treatment. *Sep. Purif. Technol.* **76**, 64–71 (2010). <https://doi.org/10.1016/j.seppur.2010.09.021>
21. R.A. Damodar, S.J. You, G.W. Chiou, Investigation on the conditions mitigating membrane fouling caused by TiO₂ deposition in a membrane photocatalytic reactor (MPR) used for dye wastewater treatment. *J. Hazard. Mater.* **203–204**, 348–356 (2012). <https://doi.org/10.1016/j.jhazmat.2011.12.027>
22. S.R. De Loos, J. Van Der Schaaf, R.M. Tiggelaar, T.A. Nijhuis, M.H.J.M. De Croon, J.C. Schouten, Gas-liquid dynamics at low Reynolds numbers in pillared rectangular micro channels. *Microfluid. Nanofluid.* **9**, 131–144 (2010). <https://doi.org/10.1007/s10404-009-0525-3>
23. A. Serizawa, Z. Feng, Z. Kawara, Two-phase flow in microchannels. *Exp. Therm. Fluid Sci.* **26**, 703–714 (2002). [https://doi.org/10.1016/S0894-1777\(02\)00175-9](https://doi.org/10.1016/S0894-1777(02)00175-9)

24. P.M.Y. Chung, M. Kawaji, The effect of channel diameter on adiabatic two-phase flow characteristics in microchannels. *Int. J. Multiphase Flow* **30**, 735–761 (2004). <https://doi.org/10.1016/j.ijmultiphaseflow.2004.05.00>
25. K.S. Elvira, R.C.R. Wootton, N.M. Reis, M.R. Mackley, A.J. DeMello, Through-wall mass transport as a modality for safe generation of singlet oxygen in continuous flows. *ACS Sustain. Chem. Eng.* **1**, 209–213 (2013). <https://doi.org/10.1021/sc300093j>
26. H. Eskandarloo, A. Badieli, M.A. Behnajady, G.M. Ziarani, UV-LEDs assisted preparation of silver deposited TiO₂ catalyst bed inside microchannels as a high efficiency microphotoreactor for cleaning polluted water. *Chem. Eng. J.* **270**, 158–167 (2015). <https://doi.org/10.1016/j.cej.2015.01.117>
27. K.N. Knust, D. Hlushkou, R.K. Anand, U. Tallarek, R.M. Crooks, Electrochemically mediated seawater desalination. *Angew. Chem. Int. Ed.* **52**, 8107–8110 (2013). <https://doi.org/10.1002/anie.201302577>
28. W. Liao, N. Wang, T. Wang, J. Xu, X. Han, Z. Liu, X. Zhang, W. Yu, Biomimetic microchannels of planar reactors for optimized photocatalytic efficiency of water purification. *Biomicrofluidics* **10**, 014123 (2016). <https://doi.org/10.1063/1.4942947>
29. A. Castedo, E. Mendoza, I. Angurell, J. Llorca, Silicone microreactors for the photocatalytic generation of hydrogen. *Catal. Today* **273**, 106–111 (2016). <https://doi.org/10.1016/j.cattod.2016.02.053>
30. O. Ola, M.M. Maroto-Valer, Synthesis, characterization and visible light photocatalytic activity of metal based TiO₂ monoliths for CO₂ reduction. *Chem. Eng. J.* **283**, 1244–1253 (2016). <https://doi.org/10.1016/j.cej.2015.07.090>
31. Z. He, Y. Li, Q. Zhang, H. Wang, Capillary microchannel-based microreactors with highly durable ZnO/TiO₂ nanorod arrays for rapid, high efficiency and continuous-flow photocatalysis. *Appl. Catal. B Environ.* **93**, 376–382 (2010). <https://doi.org/10.1016/j.apcatb.2009.10.011>
32. B.A. Marinho, R.O. Cristóvão, R. Djellabi, A. Caseiro, S.M. Miranda, J.M. Loureiro, R.A.R. Boaventura, M.M. Dias, J.C.B. Lopes, V.J.P. Vilar, Strategies to reduce mass and photons transfer limitations in heterogeneous photocatalytic processes: hexavalent chromium reduction studies. *J. Environ. Manag.* **217**, 555–564 (2018). <https://doi.org/10.1016/j.jenvman.2018.04.003>
33. S. Li, L. Yang, O. Ola, M. Maroto-Valer, X. Du, Y. Yang, Photocatalytic reduction of CO₂ by CO co-feed combined with photocatalytic water splitting in a novel twin reactor. *Energy Convers. Manag.* **116**, 184–193 (2016). <https://doi.org/10.1016/j.enconman.2016.03.001>
34. E. Baniasadi, I. Dincer, G.F. Naterer, Radiative heat transfer and catalyst performance in a large-scale continuous flow photoreactor for hydrogen production. *Chem. Eng. Sci.* **84**, 638–645 (2012). <https://doi.org/10.1016/j.ces.2012.09.013>
35. L. Ghalamchi, M.H. Rasoulifard, Immobilization of Fe₃O₄/TiO₂ nanocomposite thin layer on the glass tubes in a component parabolic collector for the treatment of DR23. *Int. J. Environ. Sci. Technol.* **16**, 7509–7522 (2019). <https://doi.org/10.1007/s13762-018-2169-x>
36. K.S. Ochoa-Gutiérrez, E. Tabares-Aguilar, M.Á. Mueses, F. Machuca-Martínez, G. Li Puma, A novel prototype offset multi tubular photoreactor (OMTP) for solar photocatalytic degradation of water contaminants. *Chem. Eng. J.* **341**, 628–638 (2018). <https://doi.org/10.1016/j.cej.2018.02.068>
37. I. Salmerón, K.V. Plakas, I. Sirés, I. Oller, M.I. Maldonado, A.J. Karabelas, S. Malato, Optimization of electrocatalytic H₂O₂ production at pilot plant scale for solar-assisted water treatment. *Appl. Catal. B Environ.* **242**, 327–336 (2019). <https://doi.org/10.1016/j.apcatb.2018.09.045>
38. A.M. Cahino, M.M.A. de Andrade, E.S. de Araújo, E.L. Silva, C. de Oliveira Cunha, E.M.R. Rocha, Degradation of tetracycline by solar photo-Fenton: optimization and application in pilot photoreactor. *Environ. Qual. Manag.* **28**, 101–106 (2018). <https://doi.org/10.1002/tqem.21579>
39. F. Cao, Q. Wei, H. Liu, N. Lu, L. Zhao, L. Guo, Development of the direct solar photocatalytic water splitting system for hydrogen production in Northwest China: design and

- evaluation of photoreactor. *Renew. Energy* **121**, 153–163 (2018). <https://doi.org/10.1016/j.renene.2018.01.016>
40. I. Boiarkina, S. Norris, D.A. Patterson, Investigation into the effect of flow structure on the photocatalytic degradation of methylene blue and dehydroabietic acid in a spinning disc reactor. *Chem. Eng. J.* **222**, 159–171 (2013). <https://doi.org/10.1016/j.cej.2013.02.025>
41. I. Boiarkina, S. Norris, D.A. Patterson, The case for the photocatalytic spinning disc reactor as a process intensification technology: comparison to an annular reactor for the degradation of methylene blue. *Chem. Eng. J.* **225**, 752–765 (2013). <https://doi.org/10.1016/j.cej.2013.03.125>
42. M. Mirzaei, B. Dabir, M. Dadvar, M. Jafarikojuour, Photocatalysis of phenol using a spinning disc photoreactor immobilized with TiO₂ nanoparticles: hydrodynamic modeling and reactor optimization. *Ind. Eng. Chem. Res.* **56**, 1739–1749 (2017). <https://doi.org/10.1021/acs.iecr.6b03204>
43. M. Mirzaei, M. Jafarikojuour, B. Dabir, M. Dadvar, Evaluation and modeling of a spinning disc photoreactor for degradation of phenol: impact of geometry modification. *J. Photochem. Photobiol. A Chem.* **346**, 206–214 (2017). <https://doi.org/10.1016/j.jphotochem.2017.05.043>
44. C. Boyle, N. Skillen, L. Stella, P.K.J. Robertson, Development and optimization of an immobilized photocatalytic system within a stacked frame photoreactor (SFPR) using light distribution and fluid mixing simulation coupled with experimental validation. *Ind. Eng. Chem. Res.* **58**, 2727–2740 (2019). <https://doi.org/10.1021/acs.iecr.8b05709>
45. M. Jafarikojuour, B. Dabir, M. Sohrabi, S.J. Royae, Application of a new immobilized impinging jet stream reactor for photocatalytic degradation of phenol: reactor evaluation and kinetic modelling. *J. Photochem. Photobiol. A Chem.* **364**, 613–624 (2018). <https://doi.org/10.1016/j.jphotochem.2018.03.043>
46. M. Jafarikojuour, B. Dabir, M. Sohrabi, S.J. Royae, Evaluation and optimization of a new design photocatalytic reactor using impinging jet stream on a TiO₂ coated disc. *Chem. Eng. Process. Process Intensif.* **121**, 215–223 (2017). <https://doi.org/10.1016/j.cep.2017.08.011>
47. M. Jafarikojuour, M. Sohrabi, S.J. Royae, M. Rezaei, A new model for residence time distribution of impinging streams reactors using descending-sized stirred tanks in series. *Chem. Eng. Res. Des.* **109**, 86–96 (2016). <https://doi.org/10.1016/j.cherd.2016.01.003>
48. Y.K. Abdel-Maksoud, E. Imam, A.R. Ramadan, TiO₂ water-bell photoreactor for wastewater treatment. *Sol. Energy* **170**, 323–335 (2018). <https://doi.org/10.1016/j.solener.2018.05.053>
49. A.A. Azzaz, A.A. Assadi, S. Jellali, S. Wolbert, S. Rtimi, L. Bousselmi, Discoloration of simulated textile effluent in continuous photoreactor using immobilized titanium dioxide: effect of zinc and sodium chloride. *J. Photochem. Photobiol. A Chem.* **358**, 111–120 (2018). <https://doi.org/10.1016/j.jphotochem.2018.01.032>
50. O. Shvydkiv, C. Limburg, K. Nolan, M. Oelgemöller, Synthesis of juglone (5-hydroxy-1,4-naphthoquinone) in a falling film microreactor. *J. Flow Chem.* **2**, 52–55 (2012). <https://doi.org/10.1556/jfchem.2012.00022>
51. S. Baghbani Ghatar, S. Allahyari, N. Rahemi, M. Tasbihi, Response surface methodology optimization for photodegradation of methylene blue in a ZnO coated flat plate continuous photoreactor. *Int. J. Chem. React. Eng.* **16**, 1–14 (2018). <https://doi.org/10.1515/ijcre-2017-0221>
52. J.C. Espíndola, R.O. Cristóvão, S.R.F. Araújo, T. Neuparth, M.M. Santos, R. Montes, J.B. Quintana, R. Rodil, R.A.R. Boaventura, V.J.P. Vilar, An innovative photoreactor, FluHelik, to promote UVC/H₂O₂ photochemical reactions: tertiary treatment of an urban wastewater. *Sci. Total Environ.* **667**, 197–207 (2019). <https://doi.org/10.1016/j.scitotenv.2019.02.335>
53. J.C. Espíndola, R.O. Cristóvão, D.A. Mayer, R.A.R. Boaventura, M.M. Dias, J.C.B. Lopes, V.J.P. Vilar, Overcoming limitations in photochemical UVC/H₂O₂ systems using a milli-photoreactor (NETmix): oxytetracycline oxidation. *Sci. Total Environ.* **660**, 982–992 (2019). <https://doi.org/10.1016/j.scitotenv.2019.01.012>
54. J.C. Espíndola, R.O. Cristóvão, S.G.S. Santos, R.A.R. Boaventura, M.M. Dias, J.C.B. Lopes, V.J.P. Vilar, Intensification of heterogeneous TiO₂ photocatalysis using the NETmix

- mili-photoreactor under microscale illumination for oxytetracycline oxidation. *Sci. Total Environ.* **681**, 467–474 (2019). <https://doi.org/10.1016/j.scitotenv.2019.05.066>
55. S.G.S. Santos, L.O. Paulista, T.F.C.V. Silva, M.M. Dias, J.C.B. Lopes, R.A.R. Boaventura, V.J.P. Vilar, Intensifying heterogeneous TiO₂ photocatalysis for bromate reduction using the NETmix photoreactor. *Sci. Total Environ.* **664**, 805–816 (2019). <https://doi.org/10.1016/j.scitotenv.2019.02.045>
56. V. Héquet, C. Raillard, O. Debono, F. Thévenet, N. Locoge, L. Le Coq, Photocatalytic oxidation of VOCs at ppb level using a closed-loop reactor: the mixture effect. *Appl. Catal. B Environ.* **226**, 473–486 (2018). <https://doi.org/10.1016/j.apcatb.2017.12.041>
57. X. Meng, N. Yun, Z. Zhang, Recent advances in computational photocatalysis: a review. *Can. J. Chem. Eng.* **97**, 1982–1998 (2019). <https://doi.org/10.1002/cjce.23477>
58. R. Acosta-Herazo, J. Monterroza-Romero, M.Á. Mueses, F. Machuca-Martínez, G. Li Puma, Coupling the six flux absorption-scattering model to the Henyey-Greenstein scattering phase function: evaluation and optimization of radiation absorption in solar heterogeneous photoreactors. *Chem. Eng. J.* **302**, 86–96 (2016). <https://doi.org/10.1016/j.cej.2016.04.127>
59. I. Rossetti, E. Bahadori, A. Tripodi, G. Ramis, Modelling of photoreactors for water treatment. *Chem. Eng. Trans.* **74**, 289–294 (2019). <https://doi.org/10.3303/CET1974049>
60. N. Padoin, C. Soares, An explicit correlation for optimal TiO₂ film thickness in immobilized photocatalytic reaction systems. *Chem. Eng. J.* **310**, 381–388 (2017). <https://doi.org/10.1016/j.cej.2016.06.013>
61. M.T. Dhotre, B. Niceno, B.L. Smith, Large eddy simulation of a bubble column using dynamic sub-grid scale model. *Chem. Eng. J.* **136**, 337–348 (2008)
62. E. Olmos, C. Gentric, C. Vial, G. Wild, N. Midoux, Numerical simulation of multiphase flow in bubble column reactors. Influence of bubble coalescence and break-up. *Chem. Eng. Sci.* **56**, 6359–6365 (2001)
63. V.K. Pareek, S.J. Cox, M.P. Brungs, B. Young, A.A. Adesina, Computational fluid dynamic (CFD) simulation of a pilot-scale annular bubble column photo-catalytic reactor. *Chem. Eng. Sci.* **58**, 859–865 (2003)
64. J. Sanyal, S. Roy, M.P. Dudukovic, Numerical simulation of gas–liquid dynamics in cylindrical bubble column reactors. *Chem. Eng. Sci.* **54**, 5071–5083 (1999)
65. M.V. Tabib, S.A. Roy, J.B. Joshi, CFD simulation of bubble column—an analysis of inter-phase forces and turbulence models. *Chem. Eng. J.* **139**, 589–614 (2008)
66. Y. Boyjoo, M. Ang, V. Pareek, CFD simulation of a pilot scale slurry photocatalytic reactor and design of multiple-lamp reactors. *Chem. Eng. Sci.* **111**, 266–277 (2014). <https://doi.org/10.1016/j.ces.2014.02.022>
67. R.L. Romero, O.M. Alfano, A.E. Cassano, Radiation field in an annular, slurry photocatalytic reactor. 2. Model and experiments. *Ind. Eng. Chem. Res.* **42**, 2479–2488 (2003)
68. J. Wang, B. Deng, J. Gao, H. Cao, Numerical simulation of radiation distribution in a slurry reactor: the effect of distribution of catalyst particles. *Chem. Eng. J.* **357**, 169–179 (2019). <https://doi.org/10.1016/j.cej.2018.09.126>
69. O.I. Tokode, R. Prabhu, L.A. Lawton, P.K.J. Robertson, Effect of controlled periodic-based illumination on the photonic efficiency of photocatalytic degradation of methyl orange. *J. Catal.* **290**, 138–142 (2012)
70. O. Tokode, R. Prabhu, L.A. Lawton, P.K.J. Robertson, Mathematical modelling of quantum yield enhancements of methyl orange photooxidation in aqueous TiO₂ suspensions under controlled periodic UV LED illumination. *Appl. Catal. B Environ.* **156–157**, 398–403 (2014)
71. O. Tokode, R. Prabhu, L.A. Lawton, P.K.J. Robertson, The effect of pH on the photonic efficiency of the destruction of methyl orange under controlled periodic illumination with UV-LED sources. *Chem. Eng. J.* **246**, 337–342 (2014)
72. C. Casado, R. Timmers, A. Sergejevs, C.T. Clarke, D.W.E. Allsopp, C.R. Bowen, R. van Grieken, J. Marugán, Design and validation of a LED-based high intensity photocatalytic reactor for quantifying activity measurements. *Chem. Eng. J.* **327**, 1043–1055 (2017). <https://doi.org/10.1016/j.cej.2017.06.167>

73. C. Casado, J. Marugán, R. Timmers, M. Muñoz, R. van Grieken, Comprehensive multiphysics modeling of photocatalytic processes by computational fluid dynamics based on intrinsic kinetic parameters determined in a differential photoreactor. *Chem. Eng. J.* **310**, 368–380 (2017). <https://doi.org/10.1016/j.cej.2016.07.081>
74. F.C. Moreira, E. Bocos, A.G.F. Faria, J.B.L. Pereira, C.P. Fonte, R.J. Santos, J.C.B. Lopes, M.M. Dias, M.A. Sanromán, M. Pazos, R.A.R. Boaventura, V.J.P. Vilar, Selecting the best piping arrangement for scaling-up an annular channel reactor: an experimental and computational fluid dynamics study. *Sci. Total Environ.* **667**, 821–832 (2019). <https://doi.org/10.1016/j.scitotenv.2019.02.260>
75. F. Denny, J. Scott, V. Pareek, G.D. Peng, R. Amal, Computational fluid dynamics modeling and optimal configuring of a channelled optical fibre photoreactor. *Chem. Eng. Sci.* **65**, 5029–5040 (2010). <https://doi.org/10.1016/j.ces.2010.06.003>
76. H. Einaga, J. Tokura, Y. Teraoka, K. Ito, Kinetic analysis of TiO₂-catalyzed heterogeneous photocatalytic oxidation of ethylene using computational fluid dynamics. *Chem. Eng. J.* **263**, 325–335 (2015). <https://doi.org/10.1016/j.cej.2014.11.017>
77. J.S. Devia-Orjuela, L.A. Betancourt-Buitrago, F. Machuca-Martinez, CFD modeling of a UV-A LED baffled flat-plate photoreactor for environment applications: a mining wastewater case. *Environ. Sci. Pollut. Res.* **26**, 4510–4520 (2019). <https://doi.org/10.1007/s11356-018-2431-2>
78. J.E. Duran, F. Taghipour, M. Mohseni, Irradiance modeling in annular photoreactors using the finite-volume method. *J. Photochem. Photobiol. A Chem.* **215**, 81–89 (2010). <https://doi.org/10.1016/j.jphotochem.2010.07.027>
79. J. Kumar, A. Bansal, Photocatalytic degradation in annular reactor: modelization and optimization using computational fluid dynamics (CFD) and response surface methodology (RSM). *J. Environ. Chem. Eng.* **1**, 398–405 (2013). <https://doi.org/10.1016/j.jece.2013.06.002>
80. J. van Walsem, S.W. Verbruggen, B. Modde, S. Lenaerts, S. Denys, CFD investigation of a multi-tube photocatalytic reactor in non-steady-state conditions. *Chem. Eng. J.* **304**, 808–816 (2016). <https://doi.org/10.1016/j.cej.2016.07.028>
81. A.J. Guadarrama-Mendoza, H.I. Villafán-Vidales, P.J. Valadés-Pelayo, C.A. Arancibia-Bulnes, D. Riveros-Rosas, H. Romero-Paredes, Radiative analysis in a multichanneled monolith solar reactor coated with ZnFe₂O₄ thin film. *Int. J. Therm. Sci.* **132**, 275–284 (2018). <https://doi.org/10.1016/j.ijthermalsci.2018.05.042>
82. A. Brucato, A.E. Cassano, F. Grisafi, G. Montante, L. Rizzuti, G. Vella, Estimating radiant fields in flat heterogeneous photoreactors by the six flux model. *AIChE J.* **52**, 3882–3890 (2006)
83. A. Brucato, L. Rizzuti, Simplified modeling of radiant fields in heterogeneous photoreactors. 1. Case of zero reflectance. *Ind. Eng. Chem. Res.* **36**, 4740–4747 (1997). <https://doi.org/10.1021/ie960259j>
84. G. Li Puma, J.N. Khor, A. Brucato, Modeling of an annular photocatalytic reactor for water purification: oxidation of pesticides. *Environ. Sci. Technol.* **38**, 3737–3745 (2004). <https://doi.org/10.1021/es0301020>
85. A. Busciglio, O.M. Alfano, F. Scargiali, A. Brucato, A probabilistic approach to radiant field modeling in dense particulate systems. *Chem. Eng. Sci.* **142**, 79–88 (2016). <https://doi.org/10.1016/j.ces.2015.11.025>
86. G. Marotta, F. Scargiali, S. Lima, G. Caputo, F. Grisafi, A. Brucato, Vacuum air-lift bioreactor for microalgae production. *Chem. Eng. Trans.* **57**, 925–930 (2017). <https://doi.org/10.3303/CET1757155>
87. G. Marotta, J. Pruvost, F. Scargiali, G. Caputo, A. Brucato, Reflection-refraction effects on light distribution inside tubular photobioreactors. *Can. J. Chem. Eng.* **95**, 1646–1651 (2017). <https://doi.org/10.1002/cjce.22811>
88. I. Grcić, G.L. Puma, Photocatalytic degradation of water contaminants in multiple photoreactors and evaluation of reaction kinetic constants independent of photon absorption, irradiance, reactor geometry and hydrodynamics. *Environ. Sci. Technol.* **47**, 13702–13711 (2013)

89. P.J. Valades-Pelayo, J. Moreira, B. Serrano, H. de Lasa, Boundary conditions and phase functions in a Photo-CREC Water-II reactor radiation field. *Chem. Eng. Sci.* **107**, 123–136 (2014)
90. R. Acosta-Herazo, M.Á. Mueses, G.L. Puma, F. Machuca-Martínez, Impact of photocatalyst optical properties on the efficiency of solar photocatalytic reactors rationalized by the concepts of initial rate of photon absorption (IRPA) dimensionless boundary layer of photon absorption and apparent optical thickness. *Chem. Eng. J.* **356**, 839–849 (2019). <https://doi.org/10.1016/j.cej.2018.09.085>
91. D. Castilla-Caballero, F. Machuca-Martínez, C. Bustillo-Lecompte, J. Colina-Márquez, Photocatalytic degradation of commercial acetaminophen: evaluation, modeling, and scaling-up of photoreactors. *Catalysts* **8**, 179 (2018). <https://doi.org/10.3390/catal8050179>
92. F. Cao, H. Li, H. Chao, L. Zhao, L. Guo, Optimization of the concentration field in a suspended photocatalytic reactor. *Energy* **74**, 140–146 (2014). <https://doi.org/10.1016/j.energy.2014.04.068>
93. M.A. Mueses, F. Machuca-Martínez, G. Li Puma, Effective quantum yield and reaction rate model for evaluation of photocatalytic degradation of water contaminants in heterogeneous pilot-scale solar photoreactors. *Chem. Eng. J.* **215–216**, 937–947 (2013). <https://doi.org/10.1016/j.cej.2012.11.076>
94. B.M. da Costa Filho, A.L.P. Araujo, S.P. Padrão, R.A.R. Boaventura, M.M. Dias, J.C.B. Lopes, V.J.P. Vilar, Effect of catalyst coated surface, illumination mechanism and light source in heterogeneous TiO₂ photocatalysis using a mili-photoreactor for n-decane oxidation at gas phase. *Chem. Eng. J.* **366**, 560–568 (2019). <https://doi.org/10.1016/j.cej.2019.02.122>
95. G. Charles, T. Roques-Carmes, N. Becheikh, L. Falk, J.M. Commenge, S. Corbel, Determination of kinetic constants of a photocatalytic reaction in micro-channel reactors in the presence of mass-transfer limitation and axial dispersion. *J. Photochem. Photobiol. A Chem.* **223**, 202–211 (2011). <https://doi.org/10.1016/j.jphotochem.2011.08.019>
96. O. Barlay Ergu, O.N. Sara, S. Yapici, M.E. Arzutug, Pressure drop and point mass transfer in a rectangular microchannel. *Int. Commun. Heat Mass Transf.* **36**, 618–623 (2009)
97. D.S. de Sá, L.E. Vasconcelos, J.R. de Souza, B.A. Marinkovic, T. Del Rosso, D. Fulvio, D. Maza, A. Massi, O. Pandoli, Intensification of photocatalytic degradation of organic dyes and phenol by scale-up and numbering-up of meso- and microfluidic TiO₂ reactors for wastewater treatment. *J. Photochem. Photobiol. A Chem.* **364**, 59–75 (2018). <https://doi.org/10.1016/j.jphotochem.2018.05.020>
98. J.R. Bolton, K.G. Bircher, W. Tumas, C.A. Tolman, Figures of merit for the technical development and application of advanced oxidation technologies for both electric and solar driven systems. *Pure Appl. Chem.* **73**, 627–637 (2001)
99. M. Compagnoni, G. Ramis, F.S. Freyria, M. Armandi, B. Bonelli, I. Rossetti, Photocatalytic processes for the abatement of N-containing pollutants from waste water. Part 1: inorganic pollutants. *J. Nanosci. Nanotechnol.* **17**, 3632–3653 (2017)
100. F.S. Freyria, M. Armandi, M. Compagnoni, G. Ramis, I. Rossetti, B. Bonelli, Catalytic and photocatalytic processes for the abatement of N-containing pollutants from wastewater. Part 2: organic pollutants. *J. Nanosci. Nanotechnol.* **17**, 3654–3672 (2017). <https://doi.org/10.1166/jnn.2017.14014>
101. F. Audino, L. Conte, A. Schenone, M. Pérez-Moya, M. Graells, O. Alfano, A kinetic study for the fenton and photo-fenton paracetamol degradation in an annular photoreactor involving assessment of LVRPA. *Environ. Sci. Pollut. Res.* **26**, 4312–4323 (2019). <https://doi.org/10.1007/s11356-018-3098-4>
102. J. Colina-Marquez, D. Castilla-Caballero, F. Machuca-Martínez, Modeling of a falling-film photocatalytic reactor: fluid dynamics for turbulent regime. *Appl. Math. Model.* **40**, 4812–4821 (2016). <https://doi.org/10.1016/j.apm.2015.12.007>